Melamine foam-supported 3D interconnected boron nitride nanosheets network encapsulated in epoxy to achieve significant thermal conductivity enhancement at an ultralow filler loading

Xiongwei Wang, Peiyi Wu

PII: S1385-8947(18)30769-1
DOI: https://doi.org/10.1016/j.cej.2018.04.196
Reference: CEJ 18996

To appear in: *Chemical Engineering Journal*

Received Date: 15 February 2018
Revised Date: 9 April 2018
Accepted Date: 27 April 2018

Please cite this article as: X. Wang, P. Wu, Melamine foam-supported 3D interconnected boron nitride nanosheets network encapsulated in epoxy to achieve significant thermal conductivity enhancement at an ultralow filler loading, *Chemical Engineering Journal* (2018), doi: https://doi.org/10.1016/j.cej.2018.04.196

Melamine foam-supported 3D interconnected boron nitride nanosheets network encapsulated in epoxy to achieve significant thermal conductivity enhancement at an ultralow filler loading

Xiongwei Wang[1], *Peiyi Wu*[1,2]*

[1]State Key Laboratory of Molecular Engineering of Polymers, Department of Macromolecular Science, Fudan University, Shanghai 200433, P. R. China

[2]State Key Laboratory for Modification of Chemical Fibers and Polymer Materials, College of Chemistry, Chemical Engineering and Biotechnology, Center for Advanced Low-Dimension Materials, Donghua University, Shanghai 201620, China

*Authors for Correspondence: peiyiwu@fudan.edu.cn

Abstract: Realizing high-efficiency thermal conductivity enhancement at low filler loading has a great significance for thermally conductive composite. Herein, three-dimensional (3D) boron nitride nanosheets (BNNSs) wrapped melamine foams (MF@BNNS) were first fabricated by repeated layer-by-layer (L-B-L) assembly using melamine skeleton as substrate and BNNSs as building blocks. The resultant MF@BNNS scaffold with order and interconnected BNNS layer, as a thermally conductive network, was further infiltrated with epoxy resin. As a consequence, a relatively high thermal conductivity of 0.6 W m^{-1} K^{-1} was achieved at an ultralow BNNS loading of ~1.1 vol%, which is equivalent to a thermal conductivity enhancement of 233 % compared to epoxy resin. Besides, the obtained epoxy composite also possesses a good mechanical property and excellent electrical insulativity. This method can be further extended to construct 3D filler network of other 2D layered

materials on the melamine foam for high-performance composite.

Keywords: thermal conductivity; layer-by-layer assembly; boron nitride; melamine foam; epoxy composite

1. Introduction

With the development of various electronic devices in the trend of higher power, miniaturization and higher integration, using high-efficiency thermal management materials has become more urgent to maintain their reliability.[1-3] Ideal thermal management materials should combine the merits of high thermal conductivity (TC), excellent electrical insulation, low cost and easy preparation.[4-7] Therefore, polymer-based thermally conductive materials show a large potential owing to their easy processing, light weight and excellent electrical insulation.[8, 9] Unfortunately, most of the neat polymers show low TC (around 0.2 W m^{-1} K^{-1}).[10, 11] For instance, the TCs of conventional epoxy thermosets are in a quite low range of 0.15-0.21 W m^{-1} K^{-1} because of their isotropic amorphous nature.[12] Although it has been reported that the formation of highly ordered structure can greatly enahnce the pristine TC of epoxy thermosets, the used epoxy monomers are high-cost and can't allow large-scale production.[12-14] Therefore, the most efficent and convenient method to enhance the polymer's TC is still focused on belnding them with many high TC but electrically insulating fillers, such as metal oxides (e.g. Al_2O_3[15-17], MgO[18, 19]), carbide (e.g. SiC[20, 21]) and metal nitride (e.g. AlN,[22, 23] BN[24-27]). Nevertheless, the impressive TC enhancement always requires a large amount of filler importation because of the low TC enhancement efficiency, which sacrifice the mechanical, processing property and meanwhile cause the high-cost.[28, 29] Therefore, obtaining a high TC enhancement at low

filler loading is of great significance but also a challenge.

A number of attempts have been made to realize the high-efficiency TC enhancement at a relatively low filler loading, such as filler functionalization[30-32], filler hybrid[33-35], rational orientation of fillers[4-8] and self-assembly into 3D filler network[11, 26, 35-38]. Recently, preforming 3D interconnected filler network as a thermally conductive path followed by vacuum-assisted impregnation of polymer has been believed a promising strategy to ensure most of the heat transfer along the filler network and finally achieve the high TC enhancement efficiency.[24] In comparison with the composite with randomly distributed fillers, this method requires an extremely low filler loading to form thermally conductive network.[36, 39] For instance, Wong et al. prepared a 3D vertically aligned and interconnected graphene network (VAIGN) via an oriented freeze-casting method for epoxy encapsulation and the obtained composite exhibited a high through-plane TC of 2.13 W m^{-1} K^{-1} at an ultralow graphene loading of 0.92 vol%.[36] Taking account of the electrically insulating property of the composite, boron nitride nanosheet (BNNS), an analogue of graphene, is another promising candidate because of its intrinsic high TC and excellent electrical insulativity.[40-44] Similarly, 3D interconnected BNNS networks encapsulated in polymer have also been investigated for the TC enhancement at low BNNS loading. For instance, Xu et al. constructed 3D-BNNS networks using ice-template approach assisted by a polymer binder (PVA) and then infiltrated them with epoxy resin to achieve a high through-plane TC of 2.85 W m^{-1} K^{-1} at a relatively low BNNSs loading of 9.29 vol%.[26] Huang et al. used cellulose nanofiber-supported 3D interconnected BNNS aerogel as a skeleton to prepare the epoxy composite with large TC enhancement of about 1400 % at a

low BNNS loading of 9.6 vol%.[24]

Although the construction of 3D filler networks can reliably realize the significant TC enhancement at low filler loading, the employed preparation methods (e. g. ice-template[11, 36, 45], chemical vapor deposition[46-48]) are always time-consumed and processing-complex, hardly meeting the requirement of large-scale production. Recently, commercial polymer foams (e. g. melamine foam, PU foam) with low density and ultrahigh porosity have been extensively investigated as the ideal substrates for the production of flexible electrode materials and water treatment materials via surface functionalization.[49-51] Liu et al. synthesize a macroscopic graphene-wrapped melamine foams (MF-G) by an MF-templated layer-by-layer (L-B-L) assembly to grow polypyrrole (PPy) for flexible supercapacitor.[49] Herein, L-B-L assembly technique enables to form an orderly and compact stacking of graphene nanosheets on the substrate, which is expected to enhance the heat transfer in the graphene layer.[52] It inspires us that by employing BNNSs as building blocks to coat them on the melamine skeleton through L-B-L assembly, it might achieve a compact and well-stacked BNNS layer around the melamine skeleton and then obtain a 3D MF-supported interconnected BNNS network. In comparison with the ice-template and chemical vapor deposition methods, this route is more facile and efficient for the construction of 3D filler network.

Herein, we reported a novel strategy for the fabrication of MF supported 3D BNNS network (MF@BNNS) via multiple L-B-L assembly using BNNS as building blocks. The resultant 3D MF@BNNS scaffold was further encapsulated by epoxy resin to obtain the epoxy composite (EP/MF@BNNS). The through-plane TC of EP/MF@BNNS composites

versus L-B-L deposition number of BNNS was investigated. As a result, a relatively high TC of 0.6 W m^{-1} K^{-1} was achieved at an ultralow BNNS loading of ~1.1 vol%, corresponding to a TC enhancement of 233 % compared to that of neat epoxy. In addition, the composite only shows a slightly decreased mechanical property but maintains an excellent electrical insulativity. These results reveal that this route can reliably realize the significant thermal conductivity enhancement for the polymer composite at an ultralow BNNS loading.

2. Experimental section

2.1. Materials

Polyethyleneimine (PEI, M_W=10000), hydrazine and *o*-dichloroaniline methane (MOCA) were purchased from Aladdin Chemical Reagent. Isopropanol (IPA) was purchased from Sinopharm Chemical Reagent Co. Ltd. (Shanghai, China). Hexagonal boron nitride powder (h-BN) was purchased from Alfa Aesar. E51 epoxy resin (EP) was provided by Bluestar Wuxi Petrochemical Co. Ltd. (Jiangsu, China). Melamine foam (MF) was purchased from local store.

2.2 Liquid exfoliation of h-BN

2 g of h-BN powders were dispersed into 200 ml IPA (50 vol%)/H_2O solution and then sonicated for 12 h to exfoliate h-BN power by a sonicator (KQ5200DB) with an output power of 250 W. Then, the dispersion was centrifuged for 30 min at 1000 rpm to separate the non-exfoliated BN, obtaining the exfoliated BNNSs.

2.3 Preparation of MF@BNNS foam

For the preparation of MF@BNNS, layer-by-layer (L-B-L) assembly method was used to coat BNNS onto the MF skeleton through the electrostatic interactions of positively charged

PEI and negatively charged BNNSs. As shown in **Fig. 1**, in a typical L-B-L assembly cycle, the fresh MF foam was firstly immersed into the PEI aqueous solution (1 mg/ml) for 2 min, rinsed several times with DI Water, and then further immersed into the BNNS dispersion (~0.5 mg/ml) in IPA (50 %)/H_2O solution for 2 min, also rinsed several times with DI water. This procedure was repeated multiple times to prepare the MF@BNNS-X foam with different L-B-L deposition cycles (X is the number of deposition cycles).

2.4 Preparation of EP/MF@BNNS composite

The EP/MF@BNNS composites were prepared via the vacuum-assisted infiltration of epoxy. First, 20.1 g of curing agent (MOCA) was homogeneously dissolved in 60 g of E51 epoxy resin monomer under vigorous stirring at 100 ^{o}C. Subsequently, the as-prepared MF@BNNS scaffold was completely immersed into the epoxy resin mixture and then transferred into a vacuum oven at 120 ^{o}C for 20 min to remove the air. After that, the resin mixture was cured at 150 ^{o}C for 2 h and 180 ^{o}C for 2.5 h. The obtained composites were denoted as EP/MF@BNNS-X, where X is the number of deposition cycles. The BNNS loading in final epoxy composite is estimated as (the subtraction of the mass of MF@BNNS and MF before and after L-B-L assembly) / (mass of the final composite after epoxy infiltration). Based on the densities of BNNS and epoxy resin, the estimated mass fraction can be further transformed to volume fraction. Moreover, EP/BNNS composites with randomly distributed BNNS were also prepared by directly adding BNNS into the epoxy resin at an identical curing process.

2.5 Characterization

The morphology of the exfoliated BNNSs was characterized by Transmission electron

microscopy (TEM) (JEOL JEM2011 F, Japan) at 200 kV. The thickness of the exfoliated BNNSs was determined by Atomic force microscopy (AFM) (Bruker Multimode 8, Germany) using the tapping mode. The cross-section morphology of the MF@BNNS scaffolds and EP/MF@BNNS composites were observed by Scanning electron microscopy (SEM) (Zeiss Ultra 55, Germany) with EDX. XRD patterns of the h-BN and exfoliated BNNSs were recorded on X'pert PRO PANalytical (Netherland) with Ni-filtered Cu Kα radiation (40 kV, 40 mA). Zeta potentials of the PEI and BNNSs were investigated on Zetasizer Nano-ZS90 (England). The hydrophilicity of the MF and MF@BNNS was characterized by the static water contact angles using OCA15 (Data-pyysics Co. Ltd., Germany). The tensile curves of the composites were measured on a universal electronic tensile machine UTM4000 (SUNS, China). The volume resistivity of the composites was measured on a Keithley Electrometer. The through-plane thermal diffusivity (α, m^2 s^{-1}) of the composites were detected by using a laser-flash diffusivity instrument LFA 447 (NETZSCH, Germany). Before the measurement, the square samples (1 cm×1 cm×1.4 mm) were firstly spray-coated with a thin layer of fine graphite powder on both sides. The density (ρ, g cm^{-3}) of a specimen was calculated by the equation: $\rho=m/v$ and the eventual thermal conductivity (λ, W m^{-1} K^{-1}) was calculated by the equation: $\lambda=\alpha \times c \times \rho$.

3. Results and discussion

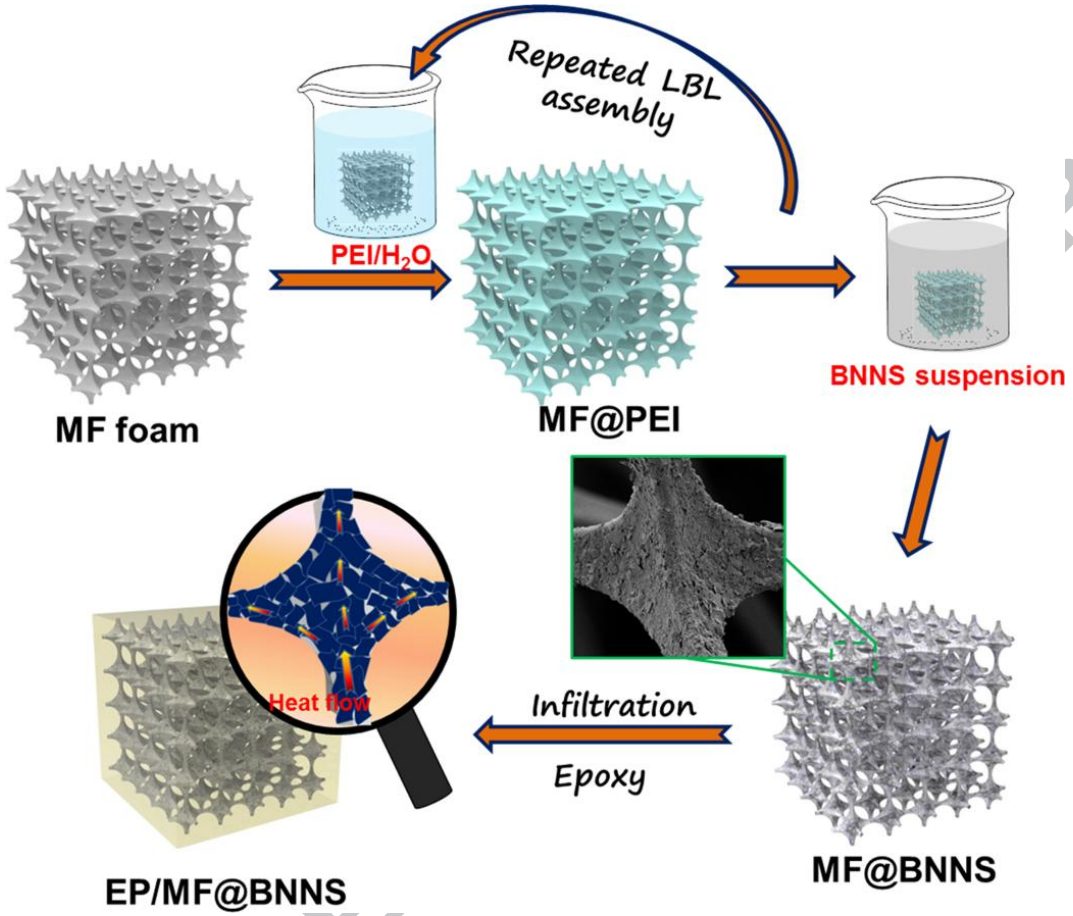

Fig. 1 Schematic illustration of the formation process of MF@BNNS foam and EP/MF@BNNS composites

The formation procedures of MF@BNNS foam and EP/MF@BNNS composite are illustrated in **Fig. 1**. Briefly, the neat MF skeleton was first wrapped by PEI/BNNS coating via the alternate deposition of anionic BNNSs and cationic PEI by a L-B-L assembly technique and then encapsulated by epoxy resin to prepare the epoxy composite. Considering the greatly larger thermal conductivity of ultrathin BNNS than that of the pristine h-BN, h-BN powder was first exfoliated to few-layered nanosheets through vigorous sonication treatment in a IPA/H_2O mixed solution. After centrifugation and collection, the morphology of the exfoliated BNNS was characterized by transmission electron microscope (TEM).

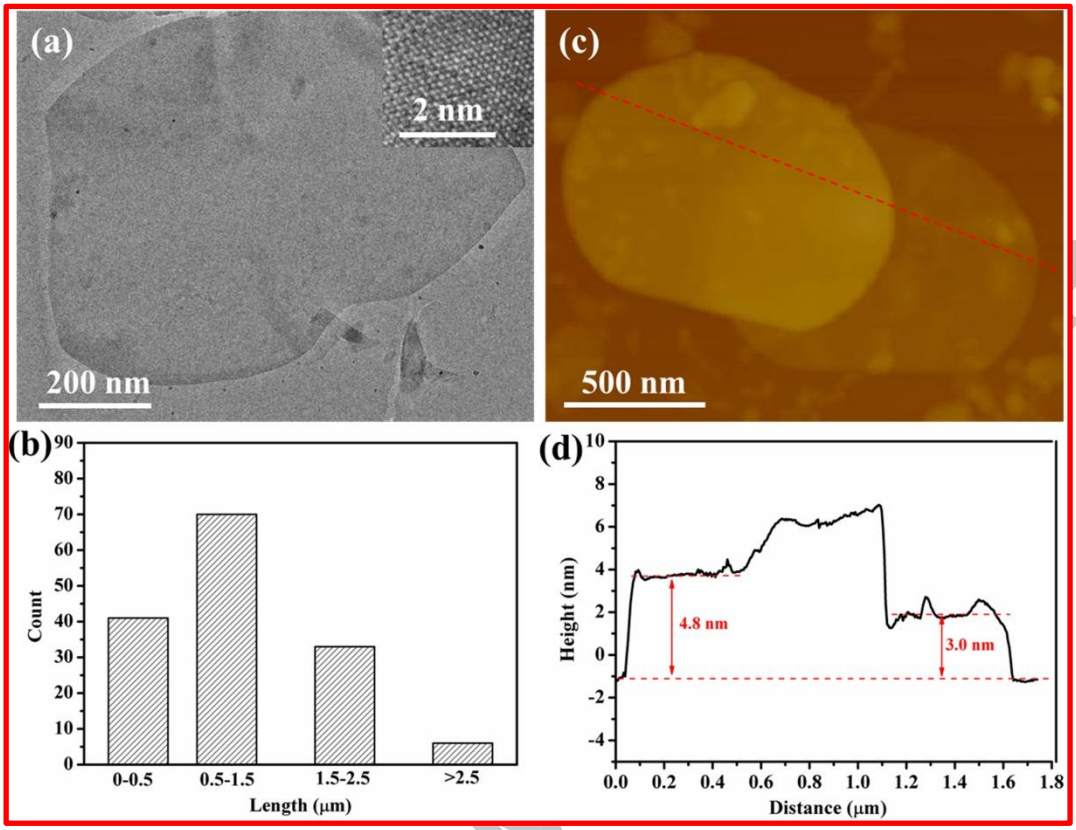

Fig. 2 (a) TEM image of exfoliated BNNSs. Inset is the high-resolution TEM image of BNNS. (b) Size statistical distribution of the exfoliated BNNS according to TEM images. AFM topography image of the exfoliated BNNSs (c) and the corresponding height curve of the exfoliated BNNS (d).

As shown in **Fig. 2**a, the obtained BNNSs show a flexible and ultrathin feature. High-resolution TEM image reveals that the BNNS still keep impeccable lattice structure after exfoliation. Furthermore, the size distribution of the exfoliated BNNSs was investigated by counting over 150 pieces of BNNSs in TEM images. One can see from **Fig. 2**b that the size of the exfoliated BNNSs is mainly distributed in the range of 0.5-1.5 μm. The large size of BNNSs is expected to reduce the interface between BNNSs along the filler network. Atomic force microscopy (AFM) was further employed to determine the thickness of the exfoliated BNNS (**Fig. 2**c). The corresponding height profile shows that the thickness of the majority of the exfoliated BNNSs is about 3-5 nm, suggesting the multilayered feature of the exfoliated BNNSs. In addition, the crystalline nature of h-BN powder and the exfoliated

BNNSs were recorded by X-ray diffraction (XRD) measurement (**Fig. S1**). The XRD pattern of h-BN and the exfoliated BNNSs both show a series of diffraction peaks, which correspond to (002), (100), (101), (102) and (004) planes, respectively.[53] After exfoliation, the peak positions of the BNNSs are almost in accord with those of pristine h-BN powder, suggesting that the hexagonal lattice is not damaged during the exfoliation process. With the (002) peak as a reference, the intensity of (100), (101), (102) and (004) diffraction peaks of BNNSs significantly decreases relative to h-BN powder, which might be attributed to the enhanced exposure of (002) plane because of the successful peel-off of few-layered BNNSs from h-BN along the (002) plane.[29, 53]

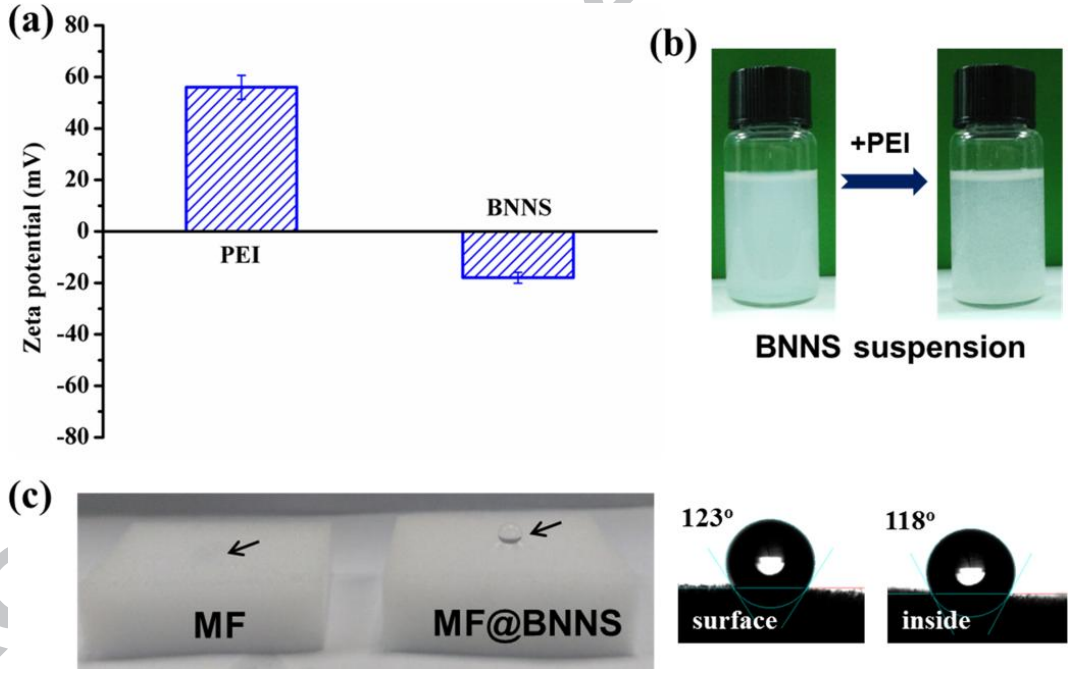

Fig. 3 (a) Zeta potential of PEI in water and BNNS in IPA/H_2O mixed solution; (b) Photograph of the BNNS dispersion before and after PEI addition; (c) Wettability of MF and MF@BNNS foams; (d) Surface and inner surface water contact angle of MF@BNNS foam

In this work, PEI and BNNS were used as the cationic and anionic adsorbent, respectively, to alternately coat them on the neat MF skeleton by a conventional L-B-L assembly technique. Therefore, the ζ potentials of cationic PEI in water and BNNSs in IPA/water mixed solution are necessary to measure. As shown in **Fig. 3**a, the ζ potential of PEI in water is around 56

mV and the ζ potential of BNNS in IPA/water is about -18 mV, suggesting the accessible electrostatic assembly of BNNS and PEI. **Fig. 3**b displays the optical pictures of BNNS suspension containing PEI or not. Without PEI, BNNSs show a homogeneous distribution with a typical Tyndall effect. The adding slight PEI, large aggregates start to form because of strong electrostatic interaction between PEI and BNNS.

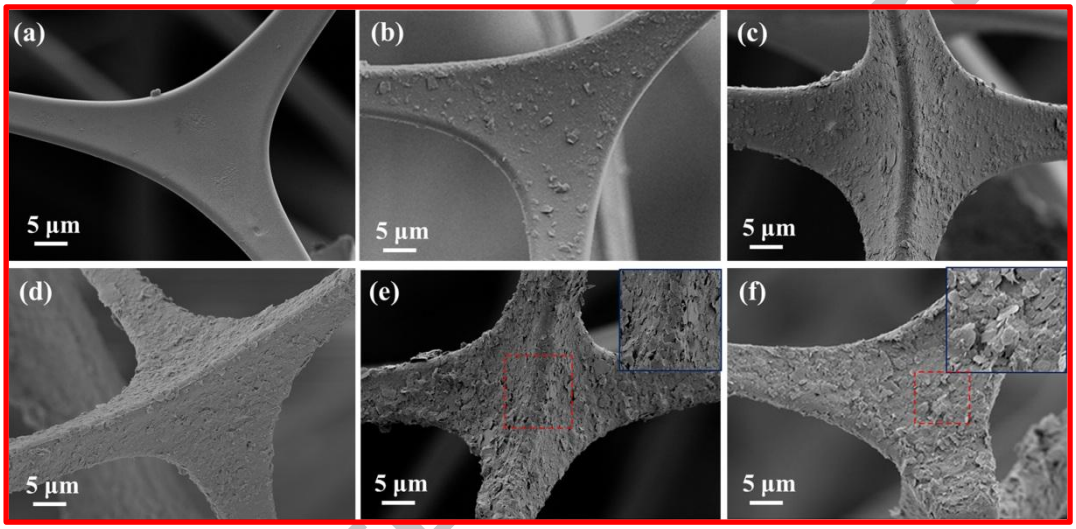

Fig. 4 SEM images of (a) MF, (b) MF@BNNS-2, (c) MF@BNNS-5, (d) MF@BNNS-10, (e) MF@BNNS-20 and (f) MF@BNNS-30. Insets show the high-magnification image.

Through alternate adsorption of cationic PEI and anionic BNNSs on MF skeleton, MF@BNNS complex foam with controllable PEI/BNNS bilayers can be achieved. As shown in **Fig. 3**c, the neat MF exhibits an open-cell microstructure with a largely hydrophilic nature for water infiltration. After coated by BNNSs, a visible hydrophilicity-hydrophobicity inversion would be triggered due to the intrinsic hydrophobicity of BNNS. The obtained MF@BNNS foam shows a large water contact angle of 123^{o} on the surface, indicating the successful coating of BNNS on the MF skeleton. When the MF@BNNS foam was cut into two pieces, the freshly cut face still exhibits a high water repellency with a water contact angle of 118^{o}, suggesting the homogeneous deposition of BNNSs throughout the cell walls. The morphology of the pristine and BNNS-modified MFs is characterized by scanning

electron microscopy (SEM). The pristine MF shows a 3D interconnected macropore structure with an average pore size of ~100 μm and a smooth surface (**Fig. 4**a and **Fig. S1**). As expected, SEM images of MF@BNNS foams show that BNNSs are tightly anchored around the cell walls of MF skeleton through the electrostatic interaction-mediated L-B-L assembly, but do not alter the open-cell microstructure of pristine MF (**Fig. 4**b-d). When the number of L-B-L deposition increases to 20 times, the BNNS plates contact and well stack one by one along the MF skeleton to form a continuous network (**Fig. 4**e). Further increase of the L-B-L cycles is expected to thicken the BNNS costing and make the thermally conductive pathways more perfect (**Fig. 4**f). The enlarged image further reveals that BNNSs have a compact stacking of their basal plane parallel to the MF surface. Importantly, the cationic PEI filled the interval between adjacent BNNSs would remove the air gaps and bridge BNNSs via electrostatic interaction, which can reduce the thermal contact resistance of adjacent BNNSs.[54] Moreover, the formation of 3D BNNS network is further elucidated by the corresponding element mapping image of element boron, which shows a homogeneous, continuous distribution throughout the MF skeleton (**Fig. 5**). Likewise, MF foam can also be closely packed by graphene nanosheets (GNSs) through the L-B-L assembly of cationic PEI and anionic graphene oxide (GO) (**Fig. S3** and **Fig. S4**). As shown in **Fig. S5**，it can be seen that the MF skeleton is homogeneously wrapped by GNSs and the increasing deposition number causes a rougher surface with a wrinkled feature.

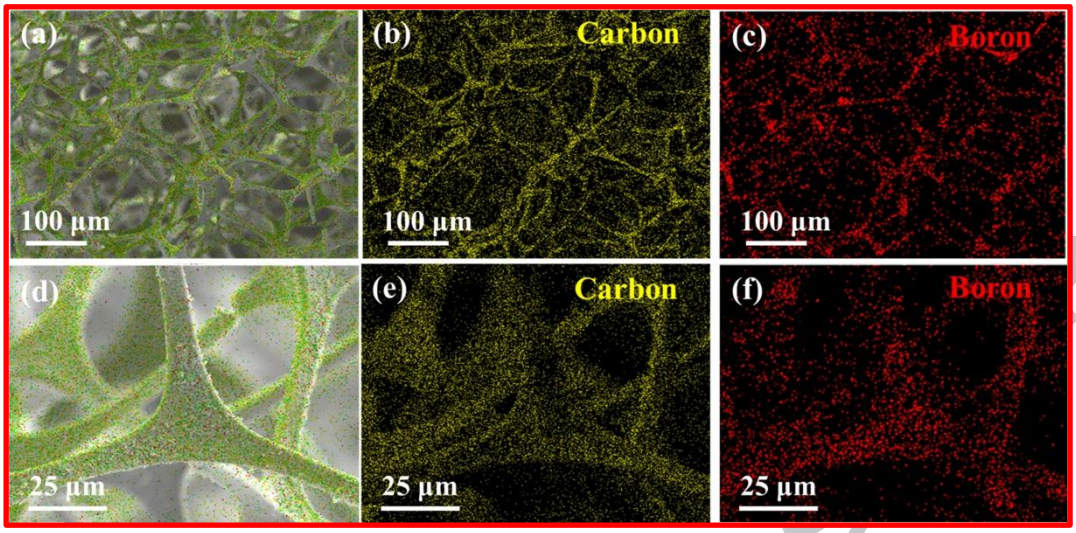

Fig. 5 Low- and high-magnification SEM image of MF@BNNS-20 (a and d) and the corresponding element mapping image of carbon (b and e) and boron (c and f).

To fabricate MF@BNNS based composites, epoxy resin with low viscosity was used to infiltrate the obtained MF@BNNS foam. **Fig. 6**a exhibits the optical image of the cured epoxy resin, EP/MF, and EP/MF@BNNS samples. One can see that the epoxy resin has a higher transmittance compared with that of the EP/MF composite. For EP/MF@BNNS composites, the transmittance is further decreased due to the incorporation of BNNS. But they still show a relatively high transmittance. In order to observe the distribution of BNNS in the epoxy matrix, the fractured surface of EP/MF@BNNS was investigated. The fractured surface of neat epoxy is very smooth owing to the high brittleness of epoxy resin (**Fig. S6**). After encapsulation by epoxy, the open pores in MF@BNNS-20 foam have been fully filled with epoxy resin, as shown in **Fig. 6**b. However, the fractured EP/MF@BNNS remain to keep a relatively smooth surface, indicating a negligible effect of MF@BNNS skeleton on the intrinsic mechanical property of epoxy matrix. Importantly, the enlarged image further shows that the 3D interconnected BNNS network is well maintained throughout the epoxy matrix, which acts as an efficient pathway for heat transfer (**Fig. 6**c-d). Furthermore, the MF@BNNS foam has a good adhesion with the epoxy resin and no obvious interfacial debonding can be

observed. This compact interface is favorable for the decrease of interface thermal resistance between BNNS and epoxy resin. On the other hand, the fractured cross-section of EP/MF@GNS composite was also investigated. **Fig. S7** shows that a continuous well-stacked GNS network is distributed at the interface between MF skeleton and epoxy resin as the highway for heat transfer.

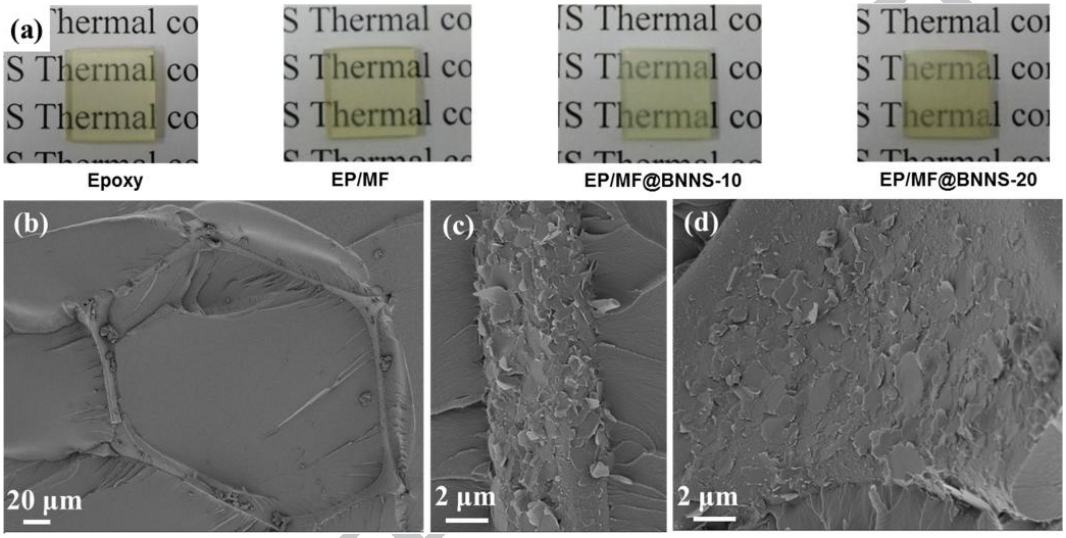

Fig. 6 (a) Photograph of epoxy, EP/MF, and EP/MF@BNNS composites. (b) low- and (c and d) high-magnification fractured surface of MF@BNNS-20 composite.

The through-plane TC of the prepared EP/MF@BNNS composites was measured by the laser-flash method at room temperature. EP/BNNS composites with randomly distributed BNNSs, as a reference, were also investigated for comparison under same conditions and its fractured surface morphology is shown in **Fig. S8**. **Fig. 7**a depicts the through-plane TC of EP/MF@BNNS composites *versus* L-B-L deposition numbers. The neat epoxy resin shows a low TC of 0.18 W m^{-1} K^{-1} due to its amorphous nature. However, the incorporation of 3D MF@BNNS framework causes a prominent increase of the TC. Below five deposition cycles, the TC of EP/MF@BNNS composites only shows a slight increase because of the insufficient

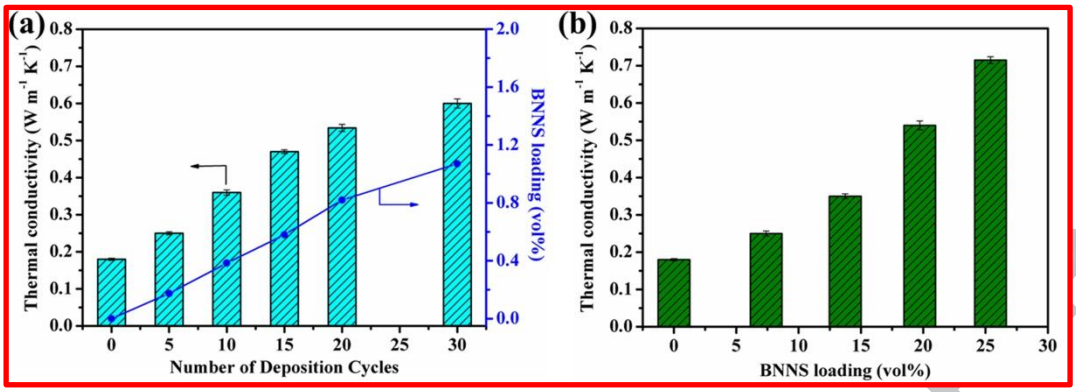

Fig. 7 (a) Through-plane TC and BNNS loading of EP/MF@BNNS composite with different L-B-L deposition number; (b) Through-plane TC of EP/BNNS composite with randomly distributed BNNS under different BNNS loading.

contact of BNNSs. As the increase of deposition cycle, TC of the composite shows a significant enhancement and a high value of 0.53 W m^{-1} K^{-1} is achieved after 20 L-B-L deposition cycles, which is nearly two times higher than that of the neat epoxy resin. These results indicate that the formation of 3D BNNS network enables to construct thermally conductive networks inside the epoxy matrix, resulting in the large enhancement of TC of the EP/MF@BNNS composite. Further increase of the deposition cycle can promote the TC (0.6 W m^{-1} K^{-1} at 30 L-B-L cycles) but the enhancement efficiency show a remarkable decrease, which is a common phenomenon for the polymer composite above the permeation threshold.[5, 55, 56] Herein, it should be noted that the BNNS content in EP/MF@BNNS-20 and EP/MF@BNNS-30 composites are estimated to be only ~0.82 and ~1.1 vol%, respectively. While for the conventional EP/BNNS composite with randomly distributed BNNSs, obtaining a similar level of TC need a higher BNNS loading above 19.7 vol%, suggesting the large superiority of preforming MF@BNNS foam as a 3D thermally conductive path on the significant enhancement of TC at a ultralow filler loading (**Fig. 7**b).[24, 55] To better compare with the previous investigations focused on the polymer/BN composites, TC enhancement per 1 vol% filler loading (η) is used to characterize the TC

Table 1 Comparison of through-plane TC and η of this work with the previously reported BN-based polymer composites.

Sample	Fill loading (vol%)	TC ($W\ m^{-1}\ K^{-1}$)	TC enhancement (%)	η	Test method	Year[Ref.]
EP/3D-C-BNNS	9.6	3.13	~1547	~161	Laser flash	2017[24]
PCL/PCL-g-BNNS	~11.2	1.01	400	~35.7	Laser flash	2016[32]
PDMS/PVA/BNNS	15.6	1.94	977	62.6	Laser flash	2017[4]
EP/BN&Fe	38.5	3.59	1690	43.9	Laser flash	2016[57]
PMMA/NF-BNNS	~69.1	10.22	4545	65.8	Laser flash	2016[29]
PEI/PI-BN	~49.1	1.7	672	13.7	Laser flash	2014[58]
TmhBN-silicone	9.2	0.58	~241	26.2	Laser flash	2015[59]
EP/VmhBN	~13.5	0.85	420	~31.1	Laser flash	2013[55]
EP/h-BN	40	9.0	~4400	~110	Laser flash	2017[25]
EP/3D-BNNS	9.3	2.4	~1100	118.3	Laser flash	2015[26]
EP/3D-BN	34	4.4	~2100	61.7	Laser flash	2017[11]
CE/BN	19.6	0.64	~156	~8.0	Steady-state	2018[60]
PA6/BNNS/graphene	~4.8	0.89	~354	~73.8	Laser flash	2016[37]
HDPE/oriented BN	~24	3.57	~865	~36	Laser flash	2017[27]
EP/MF@BNNS	~1.1	0.60	239	217.3	Laser flash	This work

enhancement efficiency of BNNSs to composites, which is defined as

$$\eta = \frac{TC - TC_0}{100VTC_0} \times 100\%$$

where TC and TC_0 represent the thermal conductivity of the composites with given BNNS content and neat polymer matrix, respectively, and V is the volume fraction of BNNS in composites. **Table 1** summarizes the η values of the previously reported polymer composites

using BNNS or h-BN as the filler. One can see that the η value in this work is higher than those of all previously reported BN-based polymer composites, to the best of our knowledge. Furthermore, compared with the fabrication of 3D porous BNNS network by ice-template or chemical vapor deposition methods, the method reported in this work is relatively much more facile and efficient. Moreover, the TC of the EP/MF@GNS composites *versus* L-B-L deposition numbers has been also investigated. As shown in **Fig. S9**, the increased deposition number of GNS is favorable to the enhancement of TC and a high TC of 0.54 W m^{-1} K^{-1} is obtained for the EP/MF@GNS composite with 10 deposition cycles. In this case, the GNS loading in EP/MF@GNS-10 composite is estimated to be 0.37 vol%, suggesting the very high TC enhancement efficiency of GNSs to composites.

To demonstrate the enhanced thermal management ability of EP/MF@BNNS composite, the surface temperature variation of the epoxy composites with time during cooling was captured by an infrared thermal camera. EP/BNNS composite with 19.7 vol% BNNS, neat epoxy, EP/MF@BNNS-10 and EP/MF@BNNS-20 composites were first placed on the same hotplate at 80 ^{o}C for 30 min to ensure uniform sample temperature, and then the surface temperature variation of these samples as a function of cooling time at room temperature environment were recorded. As shown in **Fig. 8**a, during the heat dissipation process, one can see that the EP/MF@BNNS-20 composite and EP/BNNS composite with 19.7 vol% BNNS shows much faster temperature decrease with cooling time in comparison with the neat epoxy sample because of their higher through-plane TC.

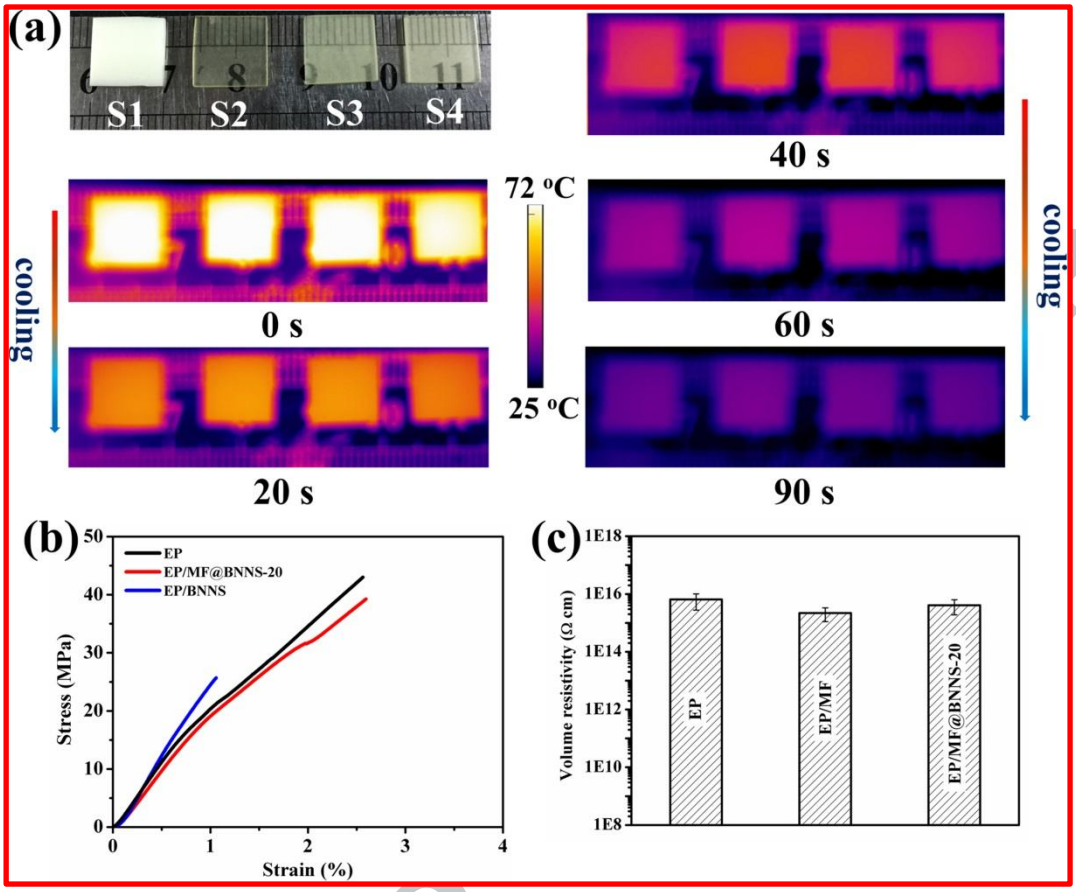

Fig. 8 (a) Infrared thermal images with cooling time of EP/BNNS composite with 19.7 vol% randomly distributed BNNS (S1), neat epoxy (S2), EP/MF@BNNS-10 composite (S3) and EP/MF@BNNS-20 composite (S4); (b) Stress-strain curves of neat epoxy, EP/MF@BNNS-20 composite and EP/BNNS composite with 19.7 vol% randomly distributed BNNS. (c) Volume resistivity of epoxy resin, EP/BNNS composite with 19.7 vol% randomly distributed BNNS and EP/MF@BNNS-20 composite.

Fig. 8b shows the tensile stress-strain curves of neat epoxy, EP/MF@BNNS-20, and EP/BNNS composite with randomly distributed BNNS. It can be seen that incorporation of MF@BNNS-20 skeleton into epoxy has a little negative effect on its mechanical property. However, at the similar level of thermal conductivity, the EP/BNNS composite with 19.7 vol% of BNNS shows a large deterioration of mechanical property owing to the serious aggregation of BNNSs and weak filler/epoxy interface adhesion. These results suggest that our method can achieve the significant TC enhancement and simultaneously maintain the good mechanical property of epoxy resin. In addition, a high enough electrical resistivity of

the heat conducting materials is important for some applications in which good electrical insulation is another key factor need to be considered. Thus the volume electrical resistivity of the neat epoxy and epoxy composites were recorded, as shown in **Fig. 8**c. In comparison with neat epoxy, incorporation of MF and MF@BNNS-20 skeletons have a negligible influence on the volume electrical resistivity of epoxy matrix. Despite this, all of them exhibit a high volume electrical resistivity over 10^{15} Ω cm, indicating an excellent electrical insulation property of them.

4. Conclusions

In summary, a novel epoxy composite with significant TC enhancement efficiency was fabricated by infiltrating 3D BNNS-wrapped melamine scaffold with epoxy resin. The 3D melamine foam supported BNNS network was first fabricated by the repeated L-B-L assembly of anionic BNNSs and cationic PEI on commercial melamine foam driven by electrostatic interaction. As a result, the obtained epoxy composite exhibits a high TC enhancement of 233 % in comparison with that of epoxy resin at an ultralow BNNS loading of 1.1 vol%. In addition, this strategy can also be extended to construct 3D interconnected graphene network on the melamine scaffold for the TC enhancement of the corresponding epoxy composite.

Acknowledgment

We gratefully acknowledge the financial support from the National Science Foundation of China (nos. 51733003, 21674025, and 51473038)

References

[1] H. Chen, V. V. Ginzburg, J. Yang, Y. Yang, W. Liu, Y. Huang, L. Du, B. Chen, Thermal conductivity of polymer-based composites: Fundamentals and applications, Prog. Polym.

Sci. 59 (2016) 41-85.
[2] A. L. Moore, L. Shi, Emerging challenges and materials for thermal management of electronics, Mater. Today 17 (2014) 163-174.
[3] X. Zeng, J. Sun, Y. Yao, R. Sun, J.-B. Xu, C.-P. Wong, A Combination of Boron Nitride Nanotubes and Cellulose Nanofibers for the Preparation of a Nanocomposite with High Thermal Conductivity, ACS Nano 11 (2017) 5167-5178.
[4] J. Chen, X. Huang, B. Sun, Y. Wang, Y. Zhu, P. Jiang, Vertically Aligned and Interconnected Boron Nitride Nanosheets for Advanced Flexible Nanocomposite Thermal Interface Materials, Acs Appl. Mater. Interfaces 9 (2017) 30909-30917.
[5] Z. Kuang, Y. Chen, Y. Lu, L. Liu, S. Hu, S. Wen, Y. Mao, L. Zhang, Fabrication of Highly Oriented Hexagonal Boron Nitride Nanosheet/Elastomer Nanocomposites with High Thermal Conductivity, Small 11 (2015) 1655-1659.
[6] X. Zhang, J. Zhang, L. Xia, J. Wang, C. Li, F. Xu, X. Zhang, H. Wu, S. Guo, Achieving high-efficiency and robust 3D thermally conductive while electrically insulating hybrid filler network with high orientation and ordered distribution, Chem. Eng. J. 334 (2018) 247-256.
[7] F. Yuan, W. Jiao, F. Yang, W. Liu, Z. Xu, R. Wang, Surface modification and magnetic alignment of hexagonal boron nitride nanosheets for highly thermally conductive composites, RSC Adv. 7 (2017) 43380-43389.
[8] X. Wang, P. Wu, Preparation of Highly Thermally Conductive Polymer Composite at Low Filler Content via a Self-Assembly Process between Polystyrene Microspheres and Boron Nitride Nanosheets, ACS Appl. Mater. Interfaces 9 (2017) 19934-19944.
[9] H. Shen, J. Guo, H. Wang, N. Zhao, J. Xu, Bioinspired Modification of h-BN for High Thermal Conductive Composite Films with Aligned Structure, ACS Appl. Mater. Interfaces 7 (2015) 5701-5708.
[10] X. Huang, C. Zhi, P. Jiang, D. Golberg, Y. Bando, T. Tanaka, Polyhedral Oligosilsesquioxane-Modified Boron Nitride Nanotube Based Epoxy Nanocomposites: An Ideal Dielectric Material with High Thermal Conductivity, Adv. Funct. Mater. 23 (2013) 1824-1831.
[11] J. Hu, Y. Huang, Y. Yao, G. Pan, J. Sun, X. Zeng, R. Sun, J.-B. Xu, B. Song, C.-P. Wong, Polymer Composite with Improved Thermal Conductivity by Constructing a Hierarchically Ordered Three-Dimensional Interconnected Network of BN, ACS Appl. Mater. Interfaces 9 (2017) 13544-13553.
[12] Y. Lin, X. Huang, J. Chen, P. Jiang, Epoxy thermoset resins with high pristine thermal conductivity, High Voltage 2 (2017) 139-146.
[13] Y.-L. Liu, Z.-Q. Cai, X. Wen, P. Pi, D. Zheng, J. Cheng, Z. Yang, Thermal properties and cure kinetics of a liquid crystalline epoxy resin with biphenyl-aromatic ester mesogen, Thermochim Acta 513 (2011) 88-93.
[14] S.-h. Song, H. Katagi, Y. Takezawa, Study on high thermal conductivity of mesogenic epoxy resin with spherulite structure, Polymer 53 (2012) 4489-4492.
[15] G. Pan, Y. Yao, X. Zeng, J. Sun, J. Hu, R. Sun, J.-B. Xu, C.-P. Wong, Learning from Natural Nacre: Constructing Layered Polymer Composites with High Thermal Conductivity, ACS Appl. Mater. Interfaces 9 (2017) 33001-33010.
[16] P. Anithambigai, M. K. D. Chakravarthii, D. Mutharasu, L. H. Huong, T. Zahner, D.

Lacey, I. Kamarulazizi, Potential thermally conductive alumina filled epoxy composite for thermal management of high power LEDs, J. Mater. Sci.-Mater. El. 28 (2017) 856-867.

[17] R. Sun, H. Yao, H. B. Zhang, Y. Li, Y. W. Mai, Z. Z. Yu, Decoration of defect-free graphene nanoplatelets with alumina for thermally conductive and electrically insulating epoxy composites, Compos. Sci. Technol. 137 (2016) 16-23.

[18] J. Zhang, Z. Du, W. Zou, H. Li, C. Zhang, MgO nanoparticles-decorated carbon fibers hybrid for improving thermal conductive and electrical insulating properties of Nylon 6 composite, Compos. Sci. Technol. 148 (2017) 1-8.

[19] H. Machrafi, G. Lebon, C.S. Iorio, Effect of volume-fraction dependent agglomeration of nanoparticles on the thermal conductivity of nanocomposites: Applications to epoxy resins, filled by SiO_2, AlN and MgO nanoparticles, Compos. Sci. Technol. 130 (2016) 78-87.

[20] J.-P. Cao, X. Zhao, J. Zhao, J.-W. Zha, G.-H. Hu, Z.-M. Dang, Improved Thermal Conductivity and Flame Retardancy in Polystyrene/Poly(vinylidene fluoride) Blends by Controlling Selective Localization and Surface Modification of SiC Nanoparticles, ACS Appl. Mater. Interfaces 5 (2013) 6915-6924.

[21] Y. Yao, X. Zeng, G. Pan, J. Sun, J. Hu, Y. Huang, R. Sun, J.-B. Xu, C.-P. Wong, Interfacial Engineering of Silicon Carbide Nanowire/Cellulose Microcrystal Paper toward High Thermal Conductivity, ACS Appl. Mater. Interfaces 8 (2016) 31248-31255.

[22] X. Huang, T. Iizuka, P. Jiang, Y. Ohki, T. Tanaka, Role of Interface on the Thermal Conductivity of Highly Filled Dielectric Epoxy/AlN Composites, J. Phys. Chem. C 116 (2012) 13629-13639.

[23] Y. Zhou, Y. Yao, C.-Y. Chen, K. Moon, H. Wang, C.-p. Wong, The use of polyimide-modified aluminum nitride fillers in AlN@PI/Epoxy composites with enhanced thermal conductivity for electronic encapsulation, Sci. Rep. 4 (2014) 4779.

[24] J. Chen, X. Huang, Y. Zhu, P. Jiang, Cellulose Nanofiber Supported 3D Interconnected BN Nanosheets for Epoxy Nanocomposites with Ultrahigh Thermal Management Capability, Adv. Funct. Mater. 27 (2017) 1604754.

[25] C. Yu, J. Zhang, Z. Li, W. Tian, L. Wang, J. Luo, Q. Li, X. Fan, Y. Yao, Enhanced through-plane thermal conductivity of boron nitride/epoxy composites, Compos. Part A-Appl. Sci. 98 (2017) 25-31.

[26] X. Zeng, Y. Yao, Z. Gong, F. Wang, R. Sun, J. Xu, C.-P. Wong, Ice-Templated Assembly Strategy to Construct 3D Boron Nitride Nanosheet Networks in Polymer Composites for Thermal Conductivity Improvement, Small 11 (2015) 6205-6213.

[27] X. Zhang, J. Zhang, L. Xia, C. Li, J. Wang, F. Xu, X. Zhang, H. Wu, S. Guo, Simple and Consecutive Melt Extrusion Method to Fabricate Thermally Conductive Composites with Highly Oriented Boron Nitrides, ACS Appl. Mater. Interfaces 9 (2017) 22977-22984.

[28] R.-C. Zhang, D. Sun, A. Lu, S. Askari, M. Macias-Montero, P. Joseph, D. Dixon, K. Ostrikov, P. Maguire, D. Mariotti, Microplasma Processed Ultrathin Boron Nitride Nanosheets for Polymer Nanocomposites with Enhanced Thermal Transport Performance, ACS Appl. Mater. Interfaces 8 (2016) 13567-13572.

[29] T. Morishita, H. Okamoto, Facile Exfoliation and Noncovalent Superacid

Functionalization of Boron Nitride Nanosheets and Their Use for Highly Thermally Conductive and Electrically Insulating Polymer Nanocomposites, ACS Appl. Mater. Interfaces 8 (2016) 27064-27073.

[30] K. Wu, J. Fang, J. Ma, R. Huang, S. Chai, F. Chen, Q. Fu, Achieving a Collapsible, Strong, and Highly Thermally Conductive Film Based on Oriented Functionalized Boron Nitride Nanosheets and Cellulose Nanofiber, ACS Appl. Mater. Interfaces 9 (2017) 30035-30045.

[31] A. Xie, Y. Wang, P. Jiang, S. Li, X. Huang, Nondestructive functionalization of carbon nanotubes by combining mussel-inspired chemistry and RAFT polymerization: Towards high dielectric nanocomposites with improved thermal management capability, Compos. Sci. Technology 154 (2018) 154-164.

[32] J. Lee, H. Jung, S. Yu, S.M. Cho, V.K. Tiwari, D.B. Velusamy, C. Park, Boron Nitride Nanosheets (BNNSs) Chemically Modified by "Grafting-From" Polymerization of Poly(caprolactone) for Thermally Conductive Polymer Composites, Chem. -Asian J. 11 (2016) 1921-1928.

[33] S.N. Leung, M.O. Khan, E. Chan, H.E. Naguib, F. Dawson, V. Adinkrah, L. Lakatos-Hayward, Synergistic effects of hybrid fillers on the development of thermally conductive polyphenylene sulfide composites, J. Appl. Polym. Sci. 127 (2013) 3293-3301.

[34] H. Ribeiro, J.P.C. Trigueiro, W.M. Silva, C.F. Woellner, P.S. Owuor, A. Cristian Chipara, M.C. Lopes, C.S. Tiwary, J.J. Pedrotti, R. Villegas Salvatierra, J.M. Tour, N. Chopra, I.N. Odeh, G.G. Silva, P.M. Ajayan, Hybrid MoS_2/h-BN Nanofillers As Synergic Heat Dissipation and Reinforcement Additives in Epoxy Nanocomposites, ACS Appl. Mater. Interfaces (2017), https://doi.org/10.1021/ acsami.7b09945.

[35] F. An, X. Li, P. Min, H. Li, Z. Dai, Z. Z. Yu, Highly anisotropic graphene/boron nitride hybrid aerogels with long-range ordered architecture and moderate density for highly thermally conductive composites, Carbon 126 (2018) 119-127.

[36] G. Lian, C. C. Tuan, L. Li, S. Jiao, Q. Wang, K.-S. Moon, D. Cui, C. P. Wong, Vertically Aligned and Interconnected Graphene Networks for High Thermal Conductivity of Epoxy Composites with Ultralow Loading, Chem. Mater. 28 (2016) 6096-6104.

[37] L. Shao, L. Shi, X. Li, N. Song, P. Ding, Synergistic effect of BN and graphene nanosheets in 3D framework on the enhancement of thermal conductive properties of polymeric composites, Compos. Sci. Technology 135 (2016) 83-91.

[38] P. Ghariniyat, S.N. Leung, Development of thermally conductive thermoplastic polyurethane composite foams via CO_2 foaming-assisted filler networking, Compos. Part B-Eng. 143 (2018) 9-18.

[39] Z. Liu, D. Shen, J. Yu, W. Dai, C. Li, S. Du, N. Jiang, H. Li, C.-T. Lin, Exceptionally high thermal and electrical conductivity of three-dimensional graphene-foam-based polymer composites, RSC Adv. 6 (2016) 22364-22369.

[40] R. Kumar, A. Parashar, Atomistic modeling of BN nanofillers for mechanical and thermal properties: a review, Nanoscale 8 (2016) 22-49.

[41] W. Luo, Y. Wang, E. Hitz, Y. Lin, B. Yang, L. Hu, Solution Processed Boron Nitride Nanosheets: Synthesis, Assemblies and Emerging Applications, Adv. Funct. Mater. 27 (2017) 1701450.

[42] W. Lei, V.N. Mochalin, D. Liu, S. Qin, Y. Gogotsi, Y. Chen, Boron nitride colloidal solutions, ultralight aerogels and freestanding membranes through one-step exfoliation and functionalization, Nat. Commun. 6 (2015) 8849.

[43] J. Yin, J. Li, Y. Hang, J. Yu, G. Tai, X. Li, Z. Zhang, W. Guo, Boron Nitride Nanostructures: Fabrication, Functionalization and Applications, Small 12 (2016) 2942-2968.

[44] X. Zhang, J. Zhang, C. Li, J. Wang, L. Xia, F. Xu, X. Zhang, H. Wu, S. Guo, Endowing the high efficiency thermally conductive and electrically insulating composites with excellent antistatic property through selectively multilayered distribution of diverse functional fillers, Chemical Engineering Journal 328 (2017) 609-618.

[45] X. Zeng, L. Ye, S. Yu, R. Sun, J. Xu, C.-P. Wong, Facile Preparation of Superelastic and Ultra low Dielectric Boron Nitride Nanosheet Aerogels via Freeze-Casting Process, Chemistry of Materials 27 (2015) 5849-5855.

[46] Y. Xue, P. Dai, M. Zhou, X. Wang, A. Pakdel, C. Zhang, Q. Weng, T. Takei, X. Fu, Z.I. Popov, P.B. Sorokin, C. Tang, K. Shimamura, Y. Bando, D. Golberg, Multifunctional Superelastic Foam-Like Boron Nitride Nanotubular Cellular-Network Architectures, ACS Nano 11 (2017) 558-568.

[47] J. Gong, Z. Liu, J. Yu, D. Dai, W. Dai, S. Du, C. Li, N. Jiang, Z. Zhan, C. T. Lin, Graphene woven fabric-reinforced polyimide films with enhanced and anisotropic thermal conductivity, Compos. Part A-Appl. Sci. 87 (2016) 290-296.

[48] Y. H. Zhao, Z. K. Wu, S. L. Bai, Thermal resistance measurement of 3D graphene foam/polymer composite by laser flash analysis, Int. J. Heat Mass Tran. 101 (2016) 470-475.

[49] L. Li, K. Wang, Z. Huang, C. Zhang, T. Liu, Highly ordered graphene architectures by duplicating melamine sponges as a three-dimensional deformation-tolerant electrode, Nano Res. 9 (2016) 2938-2949.

[50] Y. Q. Zhang, X. Bin Yang, Z. X. Wang, J. Long, L. Shao, Designing multifunctional 3D magnetic foam for effective insoluble oil separation and rapid selective dye removal for use in wastewater remediation, J.Mater. Chem. A 5 (2017) 7316-7325.

[51] L. Zhang, H. Li, X. Lai, X. Su, T. Liang, X. Zeng, Thiolated graphene-based superhydrophobic sponges for oil-water separation, Chem. Eng. J. 316 (2017) 736-743.

[52] N. Song, D. Jiao, S. Cui, X. Hou, P. Ding, L. Shi, Highly Anisotropic Thermal Conductivity of Layer-by-Layer Assembled Nanofibrillated Cellulose/Graphene Nanosheets Hybrid Films for Thermal Management, ACS Appl. Mater. Interfaces 9 (2017) 2924-2932.

[53] W. Sun, Y. Meng, Q. Fu, F. Wang, G. Wang, W. Gao, X. Huang, F. Lu, High-Yield Production of Boron Nitride Nanosheets and Its Uses as a Catalyst Support for Hydrogenation of Nitroaromatics, ACS Appl. Mater. Interfaces 8 (2016) 9881-9888.

[54] X. Zeng, L. Ye, S. Yu, H. Li, R. Sun, J. Xu, C. P. Wong, Artificial nacre-like papers based on noncovalent functionalized boron nitride nanosheets with excellent mechanical and thermally conductive properties, Nanoscale 7 (2015) 6774-6781.

[55] Z. Lin, Y. Liu, S. Raghavan, K.-s. Moon, S.K. Sitaraman, C. P. Wong, Magnetic Alignment of Hexagonal Boron Nitride Platelets in Polymer Matrix: Toward High Performance Anisotropic Polymer Composites for Electronic Encapsulation, ACS Appl.

Mater. Interfaces 5 (2013) 7633-7640.

[56] J. Gu, C. Liang, X. Zhao, B. Gan, H. Qiu, Y. Guo, X. Yang, Q. Zhang, D. Y. Wang, Highly thermally conductive flame-retardant epoxy nanocomposites with reduced ignitability and excellent electrical conductivities, Compos. Sci. Technol. 139 (2017) 83-89.

[57] S. Xu, H. Liu, Q. Li, Q. Mu, H. Wen, Influence of magnetic alignment and layered structure of BN&Fe/EP on thermal conducting performance, J. Mater. Chem. C 4 (2016) 872-878.

[58] H.L. Lee, O.H. Kwon, S.M. Ha, B.G. Kim, Y.S. Kim, J.C. Won, J. Kim, J.H. Choi, Y. Yoo, Thermal conductivity improvement of surface-enhanced polyetherimide (PEI) composites using polyimide-coated h-BN particles, Phys. Chem. Chem. Phys. 16 (2014) 20041-20046.

[59] C. Yuan, B. Duan, L. Li, B. Xie, M. Huang, X. Luo, Thermal Conductivity of Polymer-Based Composites with Magnetic Aligned Hexagonal Boron Nitride Platelets, ACS Appl. Mater. Interfaces 7 (2015) 13000-13006.

[60] Y. Li, G. Xu, Y. Guo, T. Ma, X. Zhong, Q. Zhang, J. Gu, Fabrication, proposed model and simulation predictions on thermally conductive hybrid cyanate ester composites with boron nitride fillers, Compos. Part A-Appl. Sci. 107 (2018) 570-578.

Research Highlight

1. Melamine foam was used as a substrate to deposit BNNS via layer-by-layer assembly.
2. Melamine skeleton supported 3D BNNS network was fabricated.
3. Interconnected BNNS network acts as heat transfer path in epoxy composite.
4. Significant thermal conductivity enhancement was achieved at an ultralow filler loading.

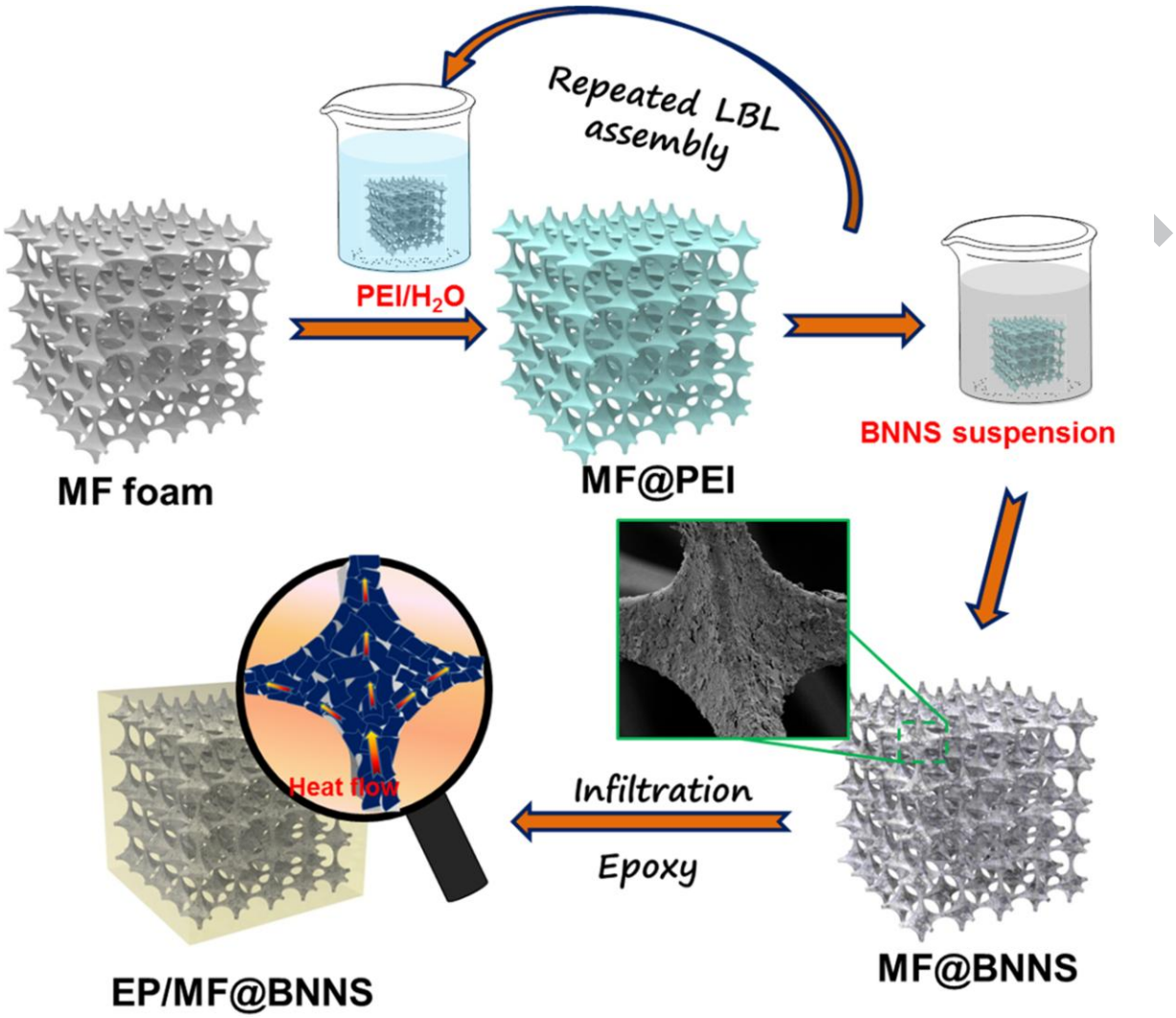
Repeated LBL assembly
PEI/H2O
MF foam
MF@PEI
BNNS suspension
MF@BNNS
Infiltration
Epoxy
Heat flow
EP/MF@BNNS